NANO LETTERS

Letter

pubs.acs.org/NanoLett

Probing Local Strain at MX_2–Metal Boundaries with Surface Plasmon-Enhanced Raman Scattering

Yinghui Sun,*[,†,#] Kai Liu,[‡,§,#] Xiaoping Hong,[†] Michelle Chen,[‡] Jonghwan Kim,[†] Sufei Shi,[†,§] Junqiao Wu,[‡,§] Alex Zettl,[†,§] and Feng Wang*[,†,§]

[†]Department of Physics and [‡]Department of Materials Science and Engineering, University of California at Berkeley, Berkeley, California 94720, United States

[§]Materials Sciences Division, Lawrence Berkeley National Laboratory, Berkeley, California 94720, United States

Supporting Information

ABSTRACT: Interactions between metal and atomically thin two-dimensional (2D) materials can exhibit interesting physical behaviors that are of both fundamental interests and technological importance. In addition to forming a metal–semiconductor Schottky junction that is critical for electrical transport, metal deposited on 2D layered materials can also generate a local mechanical strain. We investigate the local strain at the boundaries between metal (Ag, Au) nanoparticles and MX_2 (M = Mo, W; X = S) layers by exploiting the strong local field enhancement at the boundary in surface plasmon-enhanced Raman scattering (SERS). We show that the local mechanical strain splits both the in-plane vibration mode E^1_{2g} and the out-of-plane vibration mode A_{1g} in monolayer MoS_2, and activates the in-plane mode E_{1g} that is normally forbidden in backscattering Raman process. In comparison, the effects of mechanical strain in thicker MoS_2 layers are significantly weaker. We also observe that photoluminescence from the indirect bandgap transition (when the number of layers is ≥2) is quenched with the metal deposition, while a softened and broadened shoulder peak emerges close to the original direct-bandgap transition because of the mechanical strain. The strain at metal–MX_2 boundaries, which locally modifies the electronic and phonon structures of MX_2, can have important effects on electrical transport through the metal–MX_2 contact.

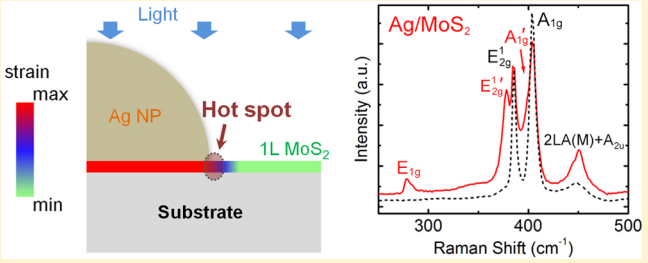

KEYWORDS: *Molybdenum disulfide, strain, Raman peak splitting, surface-enhanced Raman scattering*

Two-dimensional (2D) semiconducting transition metal dichalcogenides (MX_2), such as MoS_2 and WS_2, have recently attracted growing attention owing to their transition from an indirect bandgap in the bulk to a direct bandgap in monolayers,[1,2] and their potential applications in electronics[3,4] and photonics.[5,6] The ultrathin nature of monolayers facilitates the modulation of their physical properties by different means, such as molecular adsorption,[7,8] electric field,[3,9] and mechanical strain.[10,11] Mechanical strain is an important parameter in determining physical properties of 2D materials in high-performance devices, especially in flexible and stretchable electronics.[12−14] In-plane mechanical strain has been shown to strongly modify electronic band structure of 2D semiconductors. In monolayer MoS_2, for example, there exists a direct-to-indirect transition of the optical bandgap under a tensile strain exceeding 1%, which leads to a red shift of the photoluminescence (PL) peak and a reduction of PL intensity.[10,15−17] Moreover, strain directly modifies phonon modes in 2D materials;[10,11] a uniaxial tensile strain can readily soften the in-plane phonon vibration.[10,11,18]

Mechanical bending or stretching the substrate is typically used to control the tensile strain in 2D materials. An alternative way to introduce mechanical strain in 2D MX_2 materials is through metal deposition.[19] Probing the mechanical strain distribution at the metal–MX_2 boundary and its effect on electrical, optical, and vibrational properties of MX_2 layers are important for understanding metal–MX_2 junctions. Previous studies have shown that metal deposition can lead to significant changes in MX_2 vibrational properties,[19] but the origin of these changes is not clear. In MX_2 layers deposited with metal nanoparticles, the strain distribution is highly inhomogeneous. In order to understand optical responses of such an inhomogeneous system, careful consideration of the distribution of both mechanical strain and local optical field is crucial. Here we systematically investigate the heterosystem of deposited metal (Ag, Au) nanoparticles on 2D MX_2 (M = Mo, W; X = S) thin layers. We show that due to strongly enhanced local electric field at the metal–MX_2 boundary from surface plasmon excitation, Raman signal of the heterosystem is dominated by locally strained MX_2 layers at the boundary. The strain splits both the in-plane vibration mode E^1_{2g} and the out-of-plane vibration mode A_{1g} in monolayer MX_2 at the boundary and activates the in-plane mode E_{1g} that is normally forbidden

Received: June 25, 2014
Revised: August 12, 2014

   dx.doi.org/10.1021/nl5023767 | *Nano Lett.* XXXX, XXX, XXX–XXX

in backscattering Raman process. The splitting as well as the intensity of E_{1g} mode weakens in thicker layers. In addition, we examine PL from the metal−MX_2 system, which also has a significant component from the strained region at the boundary due to effects of surface plasmon enhancement. We find that PL from the indirect bandgap transition (when the number of layers is ≥2) is quenched, while a softened and broadened shoulder peak is observed around the original direct-bandgap transition because of strain. Our results provide a deep understanding of the plasmon-enhanced optical responses and the inhomogeneous strain distribution in metal−MX_2 systems, by the comprehensive study of the local strain effect on not only vibrational but also photoluminescence properties of metal−MX_2 with different thicknesses.

Results and Discussions. Atomically thin MoS_2 flakes were mechanically exfoliated from bulk MoS_2 crystals onto Si substrates covered with a 90 nm thick SiO_2 layer. Figure 1a shows the optical image of a local area with monolayer, bilayer, pentalayer, and bulk MoS_2. The number of layers was determined through the optical contrast, Raman, and PL spectra. The interval between Raman in-plane mode E^1_{2g} and out-of-plane mode A_{1g} can be used as an indicator of the layer number of an ultrathin exfoliated MoS_2 flake,[20,21] which is about 18 cm^{-1} in the strain-free monolayer and increases monotonically with the number of layers.[20] Figure 1b shows the representative Raman spectra excited by 488 nm laser line of mono- and few-layer MoS_2 samples. E^1_{2g} and A_{1g} modes near 400 cm^{-1} are observed. The in-plane E_{1g} mode (around 287 cm^{-1})[22] is forbidden in backscattering geometry on a basal plane due to Raman selection rules. The separations between E^1_{2g} and A_{1g} Raman peaks are 18.6 and 21.3 cm^{-1} for monolayer and bilayer (extracted by a Lorentzian peak fitting), which are consistent with reports in literatures.[20,21] Figure 1c shows the corresponding PL intensity mapping at the MoS_2 resonance energy 1.82 eV when the sample is excited by 488 nm laser. Stronger PL is detected from monolayer while much weaker PL is detected in bilayers and above because the indirect bandgap PL compared to the direct bandgap PL is a much weaker phonon-assisted process and has much smaller quantum yield. Figure 1d displays the PL spectra for different thicknesses. In the monolayer PL spectrum, the peak centered at 1.82 eV and the shoulder at 2.00 eV correspond to, respectively, the A and B direct-bandgap exciton transitions.[1] In bilayer and pentalayer, a broad PL feature from the indirect bandgap emerges, which shifts to lower energies (~1.52 eV in bilayer and ~1.37 eV in pentalayer) and become less prominent as thickness increases, also consistent with previous reports.[1]

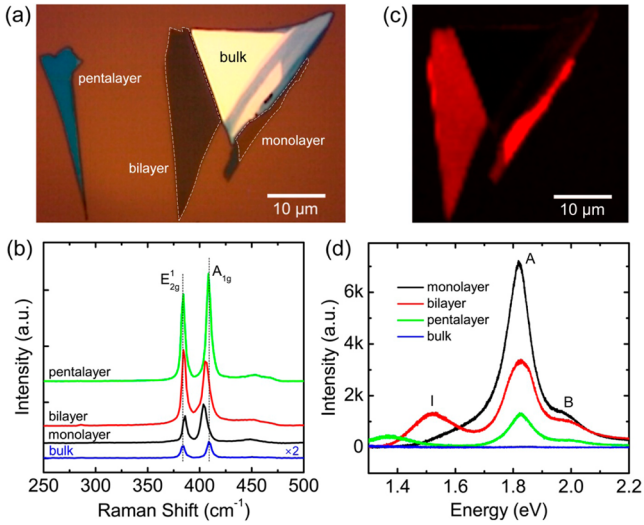

Figure 1. Optical image, Raman, and PL spectra of pristine monolayer, bilayer, and pentalayer MoS_2. (a) Optical image of exfoliated MoS_2 layers on a silicon wafer with 90 nm thick SiO_2 layer. The numbers of layers are labeled. (b) Raman spectra of MoS_2 with different layer numbers using 488 nm laser excitation. The dashed lines indicate the positions of E^1_{2g} and A_{1g} modes in bulk MoS_2, respectively. The spectra are shifted vertically for clarity. (c) PL intensity mapping at the MoS_2 resonance energy 1.82 eV when the sample is excited by a 488 nm laser. (d) PL spectra of MoS_2 with different layer numbers. A and B are the direct-bandgap transitions, and I is the indirect-bandgap transition.

Ag and Au were deposited on exfoliated MoS_2 flakes by electron beam (e-beam) evaporation with nominal thicknesses varied from 1 to 5 nm. Figure 2 shows characterization data of MoS_2 after 1 nm Ag deposition. Because Ag does not wet MoS_2, it forms nanoparticles (NPs) with an average radius of ~5 nm on MoS_2 instead of a continuous film (as shown in the AFM image in the inset of Figure 2a). Figure 2a−c shows the PL spectra of pristine and Ag-coated mono-, bi-, and pentalayer MoS_2. When the number of MoS_2 layers is ≥2, PL from an indirect bandgap transition is present in pristine MoS_2 but gets quenched after Ag deposition. However, the PL peaks from the A direct-bandgap transition (~1.82 eV) remain at the same position although with reduced intensity. The deposited metal can introduce new nonradiative recombination pathways that suppress PL emission. The indirect bandgap PL is more strongly quenched because the indirect bandgap transition in pristine sample has a much longer lifetime compared to that of the direct bandgap transition. A broadened shoulder peak centered at about 1.64 eV (extracted by a Lorentzian peak fitting and indicated by the red arrows) is observed for all Ag/MoS_2 thin-layers. This additional shoulder is more evident in the pentalayer, because the PL peak intensity of the A direct-bandgap transition is smaller than that of thinner layers. The separations between the shoulder peak and the A direct-bandgap PL are ~0.12 eV for monolayer, ~0.17 eV for bilayer, and ~0.19 eV for pentalayer.

Raman spectra for different MoS_2 layers after 1 nm Ag deposition are shown in Figure 2d−f. Compared with the Raman spectra of pristine MoS_2, E^1_{2g} and A_{1g} peaks of Ag/MoS_2 remain at the same positions. However, two new peaks redshifted from E^1_{2g} and A_{1g} modes (labeled as $E^1_{2g}{}'$ and $A_{1g}{}'$), as well as a E_{1g} peak, emerge in monolayer MoS_2 covered by Ag NPs (Figure 2d). The relative intensity of these new Raman peaks becomes much weaker in thicker MoS_2 layers (Figure 2e,f). The E_{1g} mode is inactive in the normal backscattering geometry when electric field is parallel to the MoS_2 plane. Therefore, the activation of E_{1g} peak suggests that the local electric field may develop an out-of-plane component after the Ag deposition. However, merely the change of local electric field cannot result in the new peaks of $E^1_{2g}{}'$ and $A_{1g}{}'$ modes, as well as the shoulder PL peaks around the A direct-bandgap transition. Extracted by fitting the peaks to a Lorentzian (insets of Figure 2d,e), the red shifts between $E^1_{2g}{}'$ and E^1_{2g}, $A_{1g}{}'$ and A_{1g} are, respectively, ~8.0 and ~7.9 cm^{-1} in Ag/monolayer−MoS_2, and is ~7.6 cm^{-1} between $E^1_{2g}{}'$ and E^1_{2g} in Ag/bilayer−MoS_2. The peak shifts are nearly unchanged for Ag nominal thickness ranging from 1 to 5 nm (Supporting Information Figure S1).

The observed splitting in E^1_{2g} Raman mode and a shoulder in PL spectra can be attributed to mechanical strain in MoS_2.[10,11]

dx.doi.org/10.1021/nl5023767 | Nano Lett. XXXX, XXX, XXX−XXX

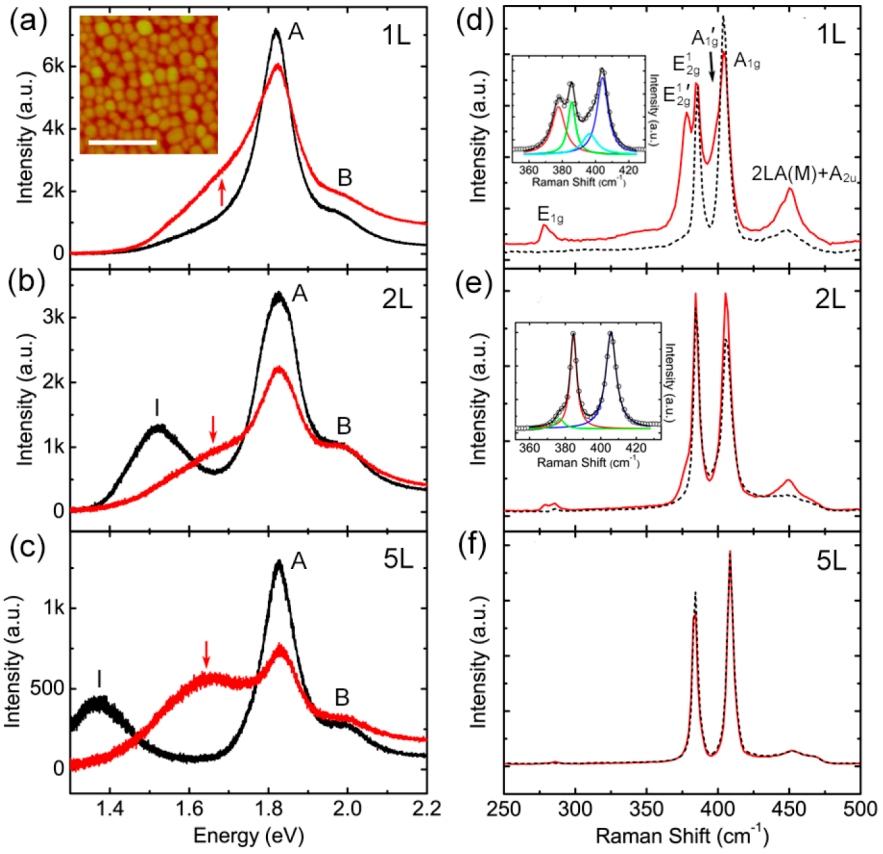

Figure 2. PL and Raman spectra of MoS_2 layers before and after 1 nm Ag deposition. (a–c) PL spectra of monolayer, bilayer, and pentalayer before (black lines) and after 1 nm Ag deposition (red lines). The red arrows indicate the positions of softened PL peaks. Inset of (a): AFM image of monolayer with Ag NPs. The scale bar is 100 nm. (d–f) Raman spectra of monolayer, bilayer, and pentalayer before (black dash lines) and after Ag deposition (red lines). The Raman modes are identified in (d). Insets: Lorentzian fitting of the splitting Raman peaks.

Similar peak splitting has also been reported in previous studies of metal-coated CVD MoS_2.[19] According to the relation between Raman shift and tensile strain,[10] the observed Raman splitting of $E_{2g}^{1\prime}$ and E_{2g}^1 at ~8 cm^{-1} in monolayer MoS_2 with Ag NPs suggests an effective strain of ~2%. The red shift of PL transition energy of MoS_2 monolayer is also consistent with a similar mechanical strain, which is ~2.6% based on the experimental relationship in literatures.[10,11] On the other hand, defects or the plasmon resonance of metal NPs might also contribute to the PL. However, the PL peaks related to defects in monolayer MoS_2 have never been observed at room temperature,[23] and the additional PL peak does not change with varying the Ag thickness (Figure 2a versus Supporting Information Figure S1d). Those exclude both factors as the dominant mechanism.

We observe similar but slightly weaker strain-induced behaviors in Raman and PL spectra in Au-MoS_2 system, where the PL from indirect-bandgap transition is quenched and the strain is estimated to be ~1.4% (Supporting Information Figure S2). Coating Ag on other 2D semiconductors, for example, exfoliated WS_2, also gives rise to very similar phenomena. As shown in Figure 3a, when excited by 488 nm laser line, the pristine monolayer WS_2 primarily shows 2LA(M), E_{2g}^1 and A_{1g} phonon modes at 351, 358, and 418 cm^{-1}, respectively. The results are consistent with reports in literatures.[24,25] After 1 nm Ag deposition, two new peaks red shifted from E_{2g}^1 and A_{1g} modes (labeled as $E_{2g}^{1\prime}$ and A_{1g}') emerge, the former of which overlaps with 2LA(M) mode.

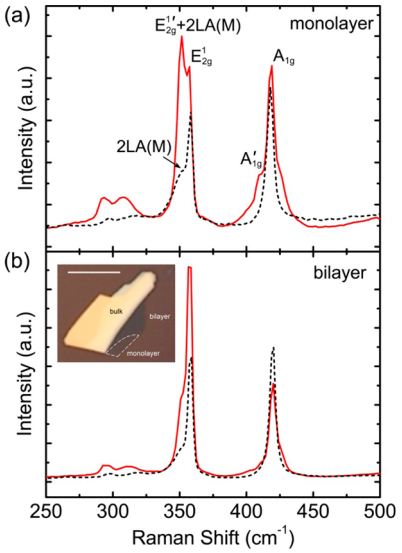

Figure 3. Raman spectra of monolayer (a) and bilayer (b) WS_2 before (black dash lines) and after (red lines) the deposition of 1 nm Ag. All spectra are collected using the 488 nm laser excitation. The Raman modes are labeled in (a). Inset: Optical image of monolayer, bilayer, and bulk WS_2 crystals on a silicon wafer with 90 nm thick SiO_2 layer. The scale bar is 10 μm.

Extracted by fitting the peaks with Lorentzians, the split between $E_{2g}^{1\prime}$ and E_{2g}^1, A_{1g}' and A_{1g} are ~5.8 and ~9.0 cm^{-1} respectively. Similar to MoS_2, the change of Raman spectrum

dx.doi.org/10.1021/nl5023767 | Nano Lett. XXXX, XXX, XXX–XXX

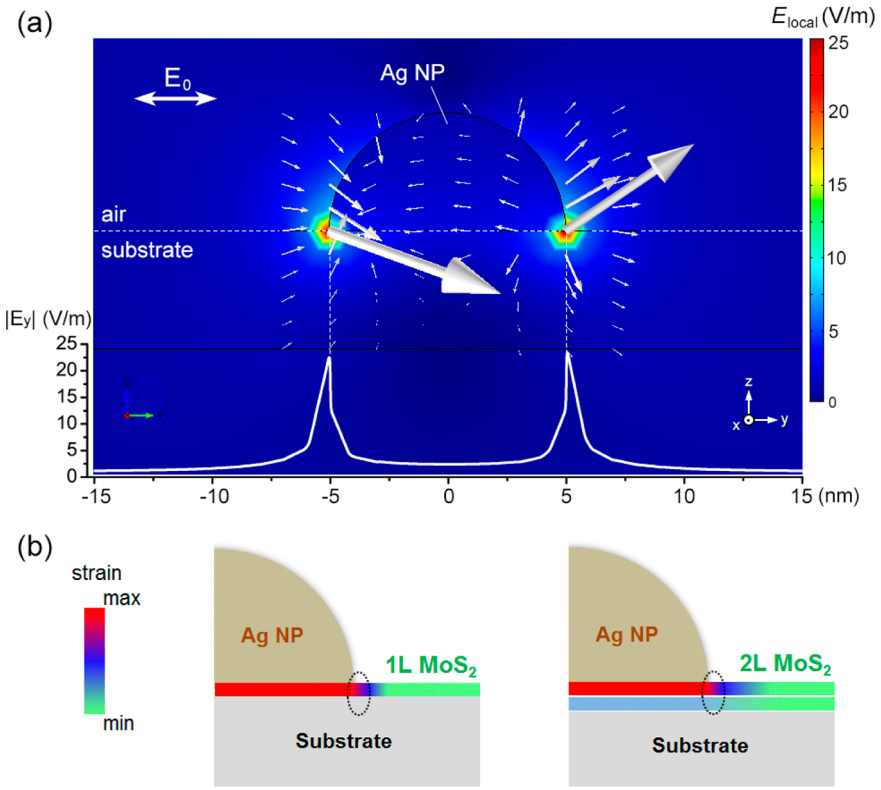

Figure 4. Distribution of the electric field and the local strain around an Ag nanoparticle. (a) Simulated distribution of the amplitude and the direction of local electric field upon an optical excitation of 488 nm wavelength. The arrows in the selected area indicate the electric field direction, and their lengths indicate the field strength. The diameter of the Ag NP is 10 nm. The polarization of incident E-field ($\boldsymbol{E}_0$) is parallel to the substrate, and its strength is set at 1 V/m. The local electric field is strongly enhanced near the Ag NP edge and has a component perpendicular to the surface of substrate. The magnitude of the in-plane electric field (E_y) along the substrate surface (dashed line) is plotted in the lower panel. (b) Schematic diagrams of the distribution of local strain in monolayer and bilayer MoS_2. The local strain in monolayer relaxes fast (left), while the local strain in the top layer of a bilayer needs more distance to relax (right). The strain in bottom layer is smaller than that in top layer. The dot circles show the positions where the large enhancement of local electric field occurs.

due to Ag nanoparticle deposition is much weaker in bilayer WS_2 (Figure 3b). These results indicate that the Raman peak splitting and shoulder peak in PL spectra induced by mechanical strain are common in Ag- or Au-coated 2D semiconductors.

With e-beam deposited Ag and Au NPs on MoS_2, several sources of stress are present. The metal nanoparticle formation follows the Volmer–Weber island growth mode.[26] Atom clusters nucleate and grow on MoS_2 surface, forming isolated metal islands. Nucleation continues to occur as long as exposed area exists. The islands keep growing until a continuous and polycrystalline film forms. However, for highly mobile materials, such as Ag and Au, the metal islands change dynamically even near room temperature, where the large islands grow at the expense of the shrinking of small islands.[26] Pashley et al. demonstrated that Ag or Au deposited on crystalline MoS_2 flake have final grain sizes larger than the initial island spacing in in situ electron microscopy studies,[27,28] revealing a liquid-like behavior of the coalescence of the initial metal nuclei. The thermodynamic driving force responsible for the surface diffusion of Ag or Au (such as surface tension) will introduce a stress between the metal and MoS_2. A strain can also be generated as the substrates cool down due to the different thermal expansion coefficients of the materials. In addition, Gong et al. proposed the lattice mismatch as the main reason for the stress built in Ag-CVD MoS_2,[19] although this effect may be less important for e-beam deposited nanoparticles due to their nonepitaxy and polycrystalline nature.

The mechanical strain in the MX_2 layers resulting from the metal–MX_2 interactions described above will be highly inhomogeneous and can vary significantly at different spatial locations. Therefore, it is surprising to observe a rather sharp splitting of the E^1_{2g} Raman mode induced by the mechanical strain in our measurements. To understand this behavior, we need to consider the Raman scattering process in this particular heterosystem. It is known that Ag and Au nanoparticles have prominent surface plasmon excitations and can lead to local electric field hot spots with strongly enhanced Raman scattering upon laser illumination. In our experiment, the reflection spectrum of Ag nanoparticles has a very broad plasmon feature centered at ~700 nm in wavelength because of the broad distribution of the particle sizes (Supporting Information Figure S3a). The low resonance energy might be ascribed to the shape of particles, which is not really spherical, and the possible surface oxidization of Ag in air. Another even more important factor determining the high local electric field at the metal–MoS_2 boundary is the lightning rod effect, where the field is dramatically enhanced around sharp edges. Therefore, both 488 and 633 nm laser lines can trigger SERS effect but with different enhancement factors (Supporting Information Figure S3b). The relatively stronger intensity of $E^1_{2g}{}'$ and $A_{1g}{}'$ peaks at the 633 nm excitation compared to their pristine counterparts indicates the dependence of local enhanced

dx.doi.org/10.1021/nl5023767 | *Nano Lett.* XXXX, XXX, XXX–XXX

Raman signal on the excitation wavelength (Supporting Information Figure S3b).

Figure 4a shows the electric field distribution around an Ag NP based on numerical simulations, where we have assumed the Ag NP to be a semisphere with a diameter of 10 nm on a SiO_2 slab. The electric field is highly localized and enhanced within ~1 nm around the circular edge of the semisphere contacting with the substrate. The maximum of local electric field E_{local}/E_0 reaches about 25, where E_0 is the strength of the incident E-field and E_{local} is the strength of the total local electric field at the presence of Ag nanostructures. The SERS enhancement factor is proportional to $(E_{local}/E_0)^4$,[29,30] which reaches up to 3.3×10^5 for the in-plane electric field in our experiment. Therefore, Raman scattering from the local area right at the metal NP−MX_2 boundary dominates the overall SERS signal. It thereby provides a unique method to probe selectively the mechanical strain at the metal−MX_2 boundaries. Experimentally we observe a similar mechanical strain effect for different Ag nanoparticle sizes (Figure 2 versus Supporting Information Figure S1). It indicates that the strain at the metal−MX_2 boundary remains largely a constant. The simulation also shows that the local electric field near the interface of Ag NP and substrate has components perpendicular to the surface of substrate. Therefore, the E_{1g} mode (around 287 cm^{-1})[22] is activated and enhanced after Ag deposition (Figure 2d,e), though it is forbidden in conventional back-scattering geometry on a basal plane. For PL emission, competing effects from local field enhancement and luminescence quenching by metal are both important. Consequently, PL from the metal−MX_2 boundary areas can still be important but will not be as dominating.

Next we examine the layer-dependent Raman spectra shown in Figure 2. According to the relationship between Raman shift and tensile strain,[10] the strains induced by Ag NPs are estimated to be about 2.1% in monolayer and 2.0% in bilayer, nearly the same values. With the increased number of layers, however, the relative intensity of Raman peak due to strain reduces dramatically. In pentalayer, there is no observable Raman signal coming from the strain. The sharp dependence of Raman signals on the number of layers is due to the distribution of the local strain (see detailed analysis in the Supporting Information), which is concentrated in the top layer. The 2D elastic modulus of bilayer MoS_2 was found to be much lower than twice the value of monolayer by nanoindentation measurements, where MoS_2 layers were probed over circular holes with merely the bottom layer being clamped by SiO_2/Si substrate around the hole edges,[31] implying the existence of an interlayer sliding as well as a weak interlayer interaction. It suggests that the friction between MoS_2 and SiO_2 is stronger than that between MoS_2 layers. In our system, therefore, monolayer MoS_2 or the bottom layer of multilayer MoS_2 can be considered to be clamped tightly by the substrate, while the top layers of multilayer MoS_2 adhere loosely to the bottom layer through weak interaction. As a result, the local load in monolayer MoS_2 will be transferred to the substrate efficiently so that the local strain relaxes in a short distance. In bilayer or multilayer MoS_2, however, the weak interlayer interaction leads to a low efficiency of load transfer from the top to the underneath layers, as well as a slower relaxation of strain in the top layer. The weak interlayer interaction leads to a weaker local strain distributed in the lower layers compared to that in the top layer. A schematic distribution of local strain is illustrated in Figure 4b. Raman signals from the less-strained or unstrained lower layers around the metal−MoS_2 interface in bilayer and multilayer MoS_2 are also locally enhanced by the plasmon resonance, and they dominate over the signal from the strained top layer (Figure 4b).

In conclusion, we have investigated the heterosystem of metal (Ag, Au)-coated MX_2 (M = Mo, W; X = S) thin layers, which exhibits a distributed mechanical strain induced by metal deposition and the local electric field. Strongly enhanced local electric field from surface plasmon excitations enables us to probe selectively the metal−MX_2 boundaries through optical methods. Raman and PL spectra show significant changes in both phonon vibrations and electronic structure at the metal−MX_2 boundary due to an induced local mechanical strain. Such local strain generation at metal−MX_2 boundaries provides a new way to engineer 2D materials and will be important to understand physical behaviors of the contact between metal and 2D semiconductors.

Experimental Section. Atomically thin MoS_2 samples of well-defined crystallographic orientation were exfoliated from bulk MoS_2 crystals onto Si substrates covered with a 90 nm thick SiO_2 layer. Single- and few-layer MoS_2 films were first identified by the optical contrast and then confirmed by the Raman spectra, where the Raman shifts of E^1_{2g} and A_{1g} depended on the layer thickness.[20,21] Raman and PL measurements were performed in air using Renishaw Invia micro-Raman system with 488 nm laser excitation. The Raman spectral resolution was ~1.5 cm^{-1}. The optical beams were focused on the sample with a spot diameter of ~2 μm. A low laser power of ~200 μW was used to prevent overheating of MoS_2. Two different metals (Ag and Au) were deposited using e-beam evaporation with 5×10^{-6} Torr base pressure. The growth morphologies of each metal were examined by atomic force microscopy (AFM), after the deposition of 1 nm thickness that was estimated by a quartz crystal oscillator. AFM measurements were performed using Veeco Multimode Atomic Force Microscope under the tapping mode.

The spatial distribution of local electric field was simulated by the finite element analysis simulations (COMSOL Multiphysics 4.3b). The Ag nanoparticle with a diameter of 10 nm on a SiO_2 slab was irradiated by the 488 nm laser. The incident electric field (plane wave) was traveling in the $-z$ direction with a polarization along the y-axis (parallels to the substrate). Perfectly matched layer with a thickness of 244 nm was set as the scattering boundary condition. The mesh size was 1 nm near the nanoparticle.

■ ASSOCIATED CONTENT

Supporting Information

(1) Optical images, Raman spectra, and PL spectra of exfoliated monolayer MoS_2 without and with 5 nm Ag deposition. (2) Raman and PL spectra of monolayer and bilayer MoS_2 with 1 nm Au deposition. (3) Reflection spectrum of Ag NPs and Raman spectra of Ag/MoS_2 at different excitation wavelengths. (4) Analysis of strain distribution in monolayer and bilayer MoS_2 coated with Ag NPs. This material is available free of charge via the Internet at http://pubs.acs.org.

■ AUTHOR INFORMATION

Corresponding Authors

*E-mail: yhsun81@gmail.com.
*E-mail: fengwang76@berkeley.edu.

dx.doi.org/10.1021/nl5023767 | Nano Lett. XXXX, XXX, XXX−XXX

Author Contributions

[#]Y.H.S. and K.L. contributed equally.

The manuscript was written through contributions of all authors. All authors have given approval to the final version of the manuscript.

Notes

The authors declare no competing financial interest.

■ ACKNOWLEDGMENTS

Y.H.S. thanks Chenhao Jin, Zhiwen Shi, and Sefaattin Tongay for helpful discussions. This work was mainly supported by Office of Basic Energy Science, Department of Energy under contract No. DE-SC0003949 (Early Career Award) and DE-AC02-05CH11231 (Materials Sciences Division). J.W. acknowledges support by the National Science Foundation under Grant DMR-1306601.

■ REFERENCES

(1) Mak, K. F.; Lee, C.; Hone, J.; Shan, J.; Heinz, T. F. *Phys. Rev. Lett.* **2010**, *105*, 136805.
(2) Splendiani, A.; Sun, L.; Zhang, Y.; Li, T.; Kim, J.; Chim, C.-Y.; Galli, G.; Wang, F. *Nano Lett.* **2010**, *10*, 1271.
(3) Radisavljevic, B.; Radenovic, A.; Brivio, J.; Giacometti, V.; Kis, A. *Nat. Nanotechnol.* **2011**, *6*, 147.
(4) Wang, Q. H.; Kalantar-Zadeh, K.; Kis, A.; Coleman, J. N.; Strano, M. S. *Nat. Nanotechnol.* **2012**, *7*, 699.
(5) Lopez-Sanchez, O.; Lembke, D.; Kayci, M.; Radenovic, A.; Kis, A. *Nat. Nanotechnol.* **2013**, *8*, 497.
(6) Yin, Z.; Li, H.; Li, H.; Jiang, L.; Shi, Y.; Sun, Y.; Lu, G.; Zhang, Q.; Chen, X.; Zhang, H. *ACS Nano* **2012**, *6*, 74.
(7) Tongay, S.; Zhou, J.; Ataca, C.; Liu, J.; Kang, J. S.; Matthews, T. S.; You, L.; Li, J.; Grossman, J. C.; Wu, J. *Nano Lett.* **2013**, *13*, 2831.
(8) Mouri, S.; Miyauchi, Y.; Matsuda, K. *Nano Lett.* **2013**, *13*, 5944.
(9) Yoon, Y.; Ganapathi, K.; Salahuddin, S. *Nano Lett.* **2011**, *11*, 3768.
(10) Conley, H. J.; Wang, B.; Ziegler, J. I.; Haglund, R. F., Jr.; Pantelides, S. T.; Bolotin, K. I. *Nano Lett.* **2013**, *13*, 3626.
(11) Zhu, C. R.; Wang, G.; Liu, B. L.; Marie, X.; Qiao, X. F.; Zhang, X.; Wu, X. X.; Fan, H.; Tan, P. H.; Amand, T.; Urbaszek, B. *Phys. Rev. B* **2013**, *88*, 121301(R).
(12) Pu, J.; Yomogida, Y.; Liu, K.-K.; Li, L.-J.; Iwasa, Y.; Takenobu, T. *Nano Lett.* **2012**, *12*, 4013.
(13) Chang, H. Y.; Yang, S. X.; Lee, J. H.; Tao, L.; Hwang, W. S.; Jena, D.; Lu, N. S.; Akinwande, D. *ACS Nano* **2013**, *7*, 5446.
(14) Yoon, J.; Park, W.; Bae, G. Y.; Kim, Y.; Jang, H. S.; Hyun, Y.; Lim, S. K.; Kahng, Y. H.; Hong, W. K.; Lee, B. H.; Ko, H. C. *Small* **2013**, *9*, 3295.
(15) Lu, P.; Wu, X.; Guo, W.; Zeng, X. C. *Phys. Chem. Chem. Phys.* **2012**, *14*, 13035.
(16) Pan, H.; Zhang, Y. W. *J. Phys. Chem. C* **2012**, *116*, 11752.
(17) Shi, H.; Pan, H.; Zhang, Y.-W.; Yakobson, B. I. *Phys. Rev. B* **2013**, *87*, 155304.
(18) He, K.; Poole, C.; Mak, K. F.; Shan, J. *Nano Lett.* **2013**, *13*, 2931.
(19) Gong, C.; Huang, C.; Miller, J.; Cheng, L.; Hao, Y.; Cobden, D.; Kim, J.; Ruoff, R. S.; Wallace, R. M.; Cho, K.; Xu, X.; Chabal, Y. J. *ACS Nano* **2013**, *7*, 11350.
(20) Lee, C.; Yan, H.; Brus, L. E.; Heinz, T. F.; Hone, J.; Ryu, S. *ACS Nano* **2010**, *4*, 2695.
(21) Hong, L.; Qing, Z.; Yap, C. C. R.; Beng Kang, T.; Edwin, T. H. J.; Olivier, A.; Baillargeat, D. *Adv. Funct. Mater.* **2012**, *22*, 1385.
(22) Wieting, T. J.; Verble, J. L. *Phys. Rev. B* **1971**, *3*, 4286.
(23) Tongay, S.; Suh, J.; Ataca, C.; Fan, W.; Luce, A.; Kang, J. S.; Liu, J.; Ko, C.; Raghunathanan, R.; Zhou, J.; Ogletree, F.; Li, J. B.; Grossman, J. C.; Wu, J. Q. *Sci. Rep.* **2013**, *3*, 2657.
(24) Gutierrez, H. R.; Perea-Lopez, N.; Elias, A. L.; Berkdemir, A.; Wang, B.; Lv, R.; Lopez-Urias, F.; Crespi, V. H.; Terrones, H.; Terrones, M. *Nano Lett.* **2013**, *13*, 3447.
(25) Berkdemir, A.; Gutierrez, H. R.; Botello-Mendez, A. R.; Perea-Lopez, N.; Elias, A. L.; Chia, C.-I.; Wang, B.; Crespi, V. H.; Lopez-Urias, F.; Charlier, J.-C.; Terrones, H.; Terrones, M. *Sci. Rep.* **2013**, *3*, 1755.
(26) Seel, S. C. Stress and Structure Evolution During Volmer-Weber Growth of Thin Films. Ph.D. Thesis, Massachusetts Institute of Technology, Cambridge, MA, 2002.
(27) Pashley, D. W.; Jacobs, M. H.; Stowell, M. J.; Law, T. J. *Philos. Mag.* **1964**, *10*, 127.
(28) Pashley, D. W.; Stowell, M. J. *J. Vac. Sci. Technol.* **1966**, *3*, 156.
(29) Xu, H. X.; Aizpurua, J.; Kall, M.; Apell, P. *Phys. Rev. E* **2000**, *62*, 4318.
(30) Le Ru, E. C.; Etchegoin, P. G. *MRS Bull.* **2013**, *38*, 631.
(31) Bertolazzi, S.; Brivio, J.; Kis, A. *ACS Nano* **2011**, *5*, 9703.